Δ isobars and nuclear saturation

A. Ekström,[1] G. Hagen,[2,3] T. D. Morris,[2,3] T. Papenbrock,[2,3] and P. D. Schwartz[2,3]
[1]*Department of Physics, Chalmers University of Technology, SE-412 96 Göteborg, Sweden*
[2]*Physics Division, Oak Ridge National Laboratory, Oak Ridge, Tennessee 37831, USA*
[3]*Department of Physics and Astronomy, University of Tennessee, Knoxville, Tennessee 37996, USA*

(Received 28 July 2017; revised manuscript received 8 December 2017; published 26 February 2018)

We construct a nuclear interaction in chiral effective field theory with explicit inclusion of the Δ-isobar Δ(1232) degree of freedom at all orders up to next-to-next-to-leading order (NNLO). We use pion-nucleon (πN) low-energy constants (LECs) from a Roy-Steiner analysis of πN scattering data, optimize the LECs in the contact potentials up to NNLO to reproduce low-energy nucleon-nucleon scattering phase shifts, and constrain the three-nucleon interaction at NNLO to reproduce the binding energy and point-proton radius of ^{4}He. For heavier nuclei we use the coupled-cluster method to compute binding energies, radii, and neutron skins. We find that radii and binding energies are much improved for interactions with explicit inclusion of Δ(1232), while Δ-less interactions produce nuclei that are not bound with respect to breakup into α particles. The saturation of nuclear matter is significantly improved, and its symmetry energy is consistent with empirical estimates.

DOI: 10.1103/PhysRevC.97.024332

I. INTRODUCTION

In recent years, *ab initio* calculation of atomic nuclei with predictive power have advanced from light [1–4] to medium-mass nuclei [5–9]. Such calculations are only as good as their input, i.e., nucleon-nucleon (NN) and three-nucleon (NNN) interactions, therefore the quest for more accurate and more precise nuclear potentials is an ongoing endeavor at the forefront of research [10–20]. Here, potentials from chiral effective field theory (χEFT)—based on long-ranged pion exchanges and short-ranged contact interactions—play a dominant role [21,22], because they are expected to deliver accuracy (via fit to data) and precision (via increasingly higher orders in the power counting). As it turns out, however, state-of-the-art χEFT potentials that are accurate for the lightest nuclei with masses $A = 2,3$ vary considerably in their saturation point for nuclear matter [14] and in their binding energy for heavier nuclei [20,23,24].

This sensitivity of the saturation point to the details of the χEFT interaction is not well understood [25] and also puzzling from an EFT perspective. A practical approach to this dilemma consists of constraining χEFT potentials to reproduce experimentally determined binding energies and charge radii of nuclei as heavy as oxygen [18]. In this work, we will follow a different approach and explicitly include the Δ isobar Δ(1232), abbreviated Δ in the following, as a low-energy degree of freedom in addition to pions (π) and nucleons (N). We recall that the Δ-N mass-splitting $\delta \equiv M_\Delta - M_N \approx 293$ MeV is roughly twice the pion mass ($M_\pi \sim 140$ MeV) and well below the expected breakdown scale of χEFT potentials [21,22]. Furthermore, the Δ also couples strongly to the πN system. For these reasons, the early chiral NN interactions [26–28] included the Δ degree of freedom. Indeed, van Kolck [26] as well as Bernard *et al.* [29] showed that the low-energy constants (LECs) of the πN interaction in a Δ-less χEFT receive a substantial contribution via resonance saturation. As nuclear interactions from χEFT with and without Δ's have a similar structure otherwise, only little effort was invested in producing quantitative Δ-full χEFT potentials. We refer the reader to the reviews [21,22] for extensive discussions of this topic.

Recently, Piarulli *et al.* [30] produced minimally nonlocal χEFT NN potentials at next-to-next-to-next-to leading order (N^{3}LO), with Δ's included up to next-to-next-to leading order (NNLO), using values for the subleading πN LECs c_1, c_2, c_3, c_4 from Ref. [31]. Dropping the nonlocal terms led to the local potentials of Ref. [32]. Two different approaches augmented these local potentials with NNN forces up to NNLO. The corresponding diagrams of the NNN force, some NN diagrams, and the most relevant LECs are shown in Fig. 1. Logoteta *et al.* [33] adjusted the LECs c_D and c_E of the short-ranged NNN terms to reproduce the saturation point of nuclear matter. However, they did not report results for few-nucleon systems. In contrast, Piarulli *et al.* [34] adjusted c_D and c_E to reproduce properties of nuclear systems with mass number $A = 3$. Their quantum Monte Carlo calculations yielded accurate results for spectra of light nuclei up to ^{12}C. We note that the potentials by Logoteta *et al.* [33] and Piarulli *et al.* [34] employ values for c_D and c_E that differ in signs and magnitudes.

In this paper we present a systematic construction and comparative analysis of nonlocal Δ-full and Δ-less χEFT potentials at LO, NLO, and NNLO, and report results for light- and medium-mass nuclei, and infinite nucleonic matter. We constrain the relevant short-ranged LECs using experimental data from nuclear systems with mass numbers $A = 2,4$ and use πN LECs determined in a recent high-precision analysis [37] based on the Roy-Steiner equations [38]. We do not include any additional contact operators beyond NNLO in Weinberg power counting. We find that the resulting Δ-full potentials yield accurate charge radii and much improved binding energies for medium mass nuclei, and reproduce the saturation point

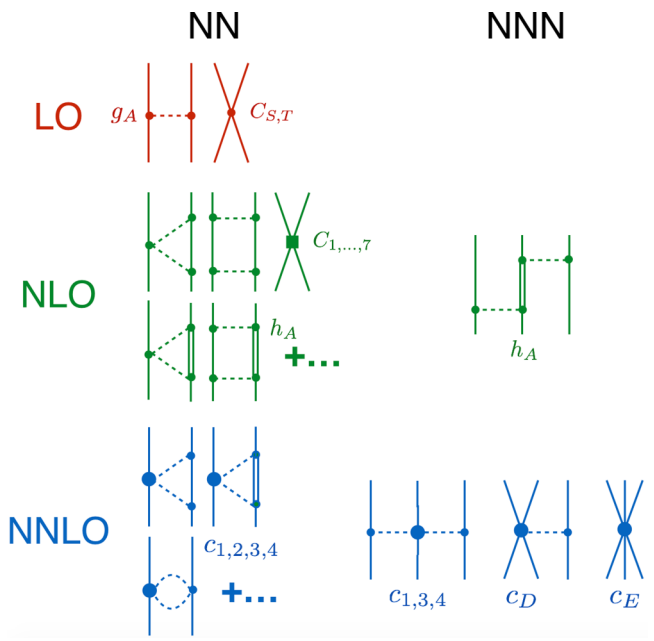

FIG. 1. Schematic figure of relevant diagrams that enter in Δ-full χEFT at leading order (LO), next-to-leading order (NLO), and next-to-next-to-leading order (NNLO). The leading πN and $\pi N\Delta$ axial couplings are denoted by g_A and h_A, respectively. Note that there are no Δ contributions at LO. At NLO, the *NN* contact interactions also remain unchanged. However, the leading-order *NNN* interaction, i.e., the well-known Fujita-Miyazawa term [35], appears at this order; see also Ref. [36]. The Δ contributions to the *NNN* interaction at NNLO vanish because of the Pauli principle or are suppressed and demoted to a higher chiral order. In addition to the subleading πN LECs c_1,c_2,c_3,c_4, the *NNN* diagrams contain two additional LECs: c_D and c_E.

of symmetric nuclear matter within estimated EFT-truncation errors. Furthermore, estimates of the EFT-truncation errors furnish a discussion of the improved convergence rate of the Δ-full χEFT expansion compared to the Δ-less theory.

II. OPTIMIZATION OF INTERACTIONS

To isolate the effects of the Δ isobar in the description of the saturation properties of nucleonic matter we compare our results with Δ-less χEFT potentials at LO, NLO, and NNLO. Other than the inclusion of the Δ isobar, the Δ-full and the Δ-less interactions are constructed following identical optimization protocols. For the description of the interaction we build on work [26,31,36,39,40] and treat the Δ-*N* mass difference $\delta \equiv M_\Delta - M_\mathrm{N}$ as an additional small scale. A power counting for this approach is provided by the so-called small-scale expansion [39]. This is identical to the conventional heavy-baryon formulation of χEFT which is already used for including the nucleon mass scale without any Δ isobars. The Δ-less pion exchanges in the *NN* sector up to NNLO are given in Ref. [16]. The expressions for the *NN* contact potentials at LO and NLO are given in, e.g., Ref. [22], and the Δ contributions to the leading and subleading 2π exchanges in the *NN* potential are from Ref. [31]. Charge-independence breaking terms are included in the LO contact LECs as well as the one-pion exchange. Following Ref. [41] we remove all contributions that are proportional to the subleading $\pi N\Delta$ coupling $b_3 + b_8$ by renormalizing the $\pi N\Delta$ axial coupling h_A and the subleading πN couplings $c_{2,3,4}$. We follow Siemens *et al.* [37] and use $h_A = 1.40$, $g_A = 1.289$, and the central Roy-Steiner values of the πN LECs for the Δ-full and Δ-less potentials up to third order. We recall that Δ-less χEFT potentials often employ πN LECs with values that differ from what is found in πN scattering, because the absence of Δ's strongly renormalize the πN couplings $c_{2,3,4}$ in the three-nucleon sector [42]. The Δ-full theory is more consistent in this regard and the c_i's appear to be more natural in size.

The expressions for the three-nucleon diagrams at NNLO are from Ref. [11]. The NLO *NNN* force in the Δ-full theory is given by the well-known Fujita-Miyazawa term [35]. This topology is identical in structure to the Δ-less 2π-exchange *NNN* interaction when using the resonance-saturation values for the relevant πN LECs,

$$c_3^\Delta = -2c_4^\Delta = \frac{4h_A^2}{9\delta} = -2.972246\ \mathrm{GeV}^{-1}.$$

To construct quantitative Δ-full χEFT potentials we need to determine the numerical values of the LECs in the LO and NLO contact potentials and the c_D and c_E terms in the *NNN* interaction at NNLO. To optimize the contact LECs we use a Levenberg-Marquardt algorithm with machine-precise derivatives from automatic differentiation [20]. The objective function for the LO and NLO contact LECs consists of the sum of squared differences between the theoretical partial-wave *NN* scattering phase shifts and the corresponding values from the Granada analysis [43] up to 200-MeV scattering energy in the laboratory system. At LO, we only use phase shifts up to 1 MeV. The neutron-neutron LEC $\tilde{C}^{(nn)}_{^1S_0}$ is constrained to reproduce the effective range expansion in the $^1S_0$ channel. At NNLO we use the same optimization algorithm to find the c_D and c_E LECs that simultaneously reproduce the binding energy and point-proton radius of ^{4}He. Although correlated, these $A = 4$ observables provide enough information to identify a unique minimum in the c_D-c_E plane that is sufficient for the purpose of comparing the effects in nuclei and nucleonic matter from the Δ isobar. An extended regression analysis or Bayesian inference approach including additional data from many-nucleon systems or three-nucleon scattering would generate interactions for use in detailed analyses of atomic nuclei or model selection. In this work we focus on the effects of the Δ isobar in nucleonic matter.

To regulate the the interactions we use the usual nonlocal regulators,

$$f(p) = \exp\left[-\left(\frac{p^2}{\Lambda^2}\right)^3\right],$$

$$f(p,q) = \exp\left[-\left(\frac{4p^2+3q^2}{4\Lambda^2}\right)^3\right],$$

in the *NN* and *NNN* interactions, respectively. Here, p and q denote the Jacobi momenta in the two-body system and spectator nucleon, respectively, and Λ is the momentum cutoff.

TABLE I. Numerical values of the LECs for Δ-full χEFT potentials with a momentum cutoff $\Lambda = 450$ MeV at LO, NLO, and NNLO. The πN LECs $c_{1,2,3,4}$ are taken from the Roy-Steiner analysis in Ref. [37], and for consistency we use $h_A = 1.40$, $g_A = 1.289$, and $F_\pi = 92.2$ MeV.

LEC	LO(450)	ΔNLO(450)	ΔNNLO(450)	LO(500)	ΔNLO(500)	ΔNNLO(500)
c_1	–	–	−0.74	–	–	−0.74
c_2	–	–	−0.49	–	–	−0.49
c_3	–	–	−0.65	–	–	−0.65
c_4	–	–	+0.96	–	–	+0.96
$\tilde{C}_{^1S_0}^{(nn)}$	−0.112 927	−0.310 511	−0.338 023	−0.108 522	−0.310 256	−0.338 223
$\tilde{C}_{^1S_0}^{(np)}$	−0.112 927	−0.310 712	−0.338 139	−0.108 522	−0.310 443	−0.338 320
$\tilde{C}_{^1S_0}^{(pp)}$	−0.112 927	−0.309 893	−0.337 137	−0.108 522	−0.309 618	−0.337 303
$\tilde{C}_{^3S_1}$	−0.087 340	−0.197 951	−0.229 310	−0.068 444	−0.191 013	−0.221 721
$C_{^1S_0}$	–	+2.391 638	+2.476 589	–	+2.395 375	+2.488 019
$C_{^3S_1}$	–	+0.558 973	+0.695 953	–	+0.539 378	+0.675 353
$C_{^1P_1}$	–	+0.004 813	−0.028 541	–	+0.015 247	−0.012 651
$C_{^3P_0}$	–	+0.686 902	+0.645 550	–	+0.727 049	+0.698 454
$C_{^3P_1}$	–	−1.000 112	−1.022 359	–	−0.951 417	−0.937 264
$C_{^3P_2}$	–	−0.808 073	−0.870 203	–	−0.793 621	−0.859 526
$C_{^3S_1-^3D_1}$	–	+0.362 094	+0.358 330	–	+0.358 443	+0.354 479
c_D	–	–	+0.790	–	–	−0.820
c_E	–	–	+0.017	–	–	−0.350

The nonlocal regulator acts multiplicative, i.e.,

$$V_{NN}(p',p) \to f(p')V_{NN}(p',p)f(p),$$
$$V_{NNN}(p',q';p,q) \to f(p',q')V_{NNN}(p',q';p,q)f(p,q).$$

To explore the sensitivity of the results with respect to changes in the cutoff Λ we employ two common choices, namely $\Lambda = 450$ MeV and $\Lambda = 500$ MeV. To regularize the 2π exchanges in conjunction with nonlocal regulation we use the standard spectral-function regularization (SFR) [44] with a cutoff $\tilde{\Lambda} = 700$ MeV throughout. It should also be pointed out that recent work, e.g., Refs. [45–47], indicates that a carefully selected local regulation of the long-ranged 2π exchanges render SFR redundant and yields an improved analytical structure of the scattering amplitude. However, the overall existence of such scheme dependencies [48] will persist as long as the chiral interactions cannot be order-by-order renormalized; see, e.g., Ref. [49] for a recent analysis. The numerical values of the employed πN LECs and the optimized short-ranged LECs for the Δ-less as well as the Δ-full potentials are given in Tables I and II. For the masses of the pions ($\pi^{\pm,0}$), proton, neutron, nucleon (p,n,N), and Δ we use the following

TABLE II. Numerical values of the LECs for Δ-less χEFT potentials with a momentum cutoff $\Lambda = 500$ MeV at LO, NLO, and NNLO. The πN LECs $c_{1,3,4}$ are taken from the Roy-Steiner analysis in Ref. [37], and for consistency we use $g_A = 1.289$, and $F_\pi = 92.2$ MeV.

LEC	LO(450)	NLO(450)	NNLO(450)	LO(500)	NLO(500)	NNLO(500)
c_1	–	–	−0.74	–	–	−0.74
c_3	–	–	−3.61	–	–	−3.61
c_4	–	–	+2.44	–	–	+2.44
$\tilde{C}_{^1S_0}^{(nn)}$	−0.112 927	−0.149 559	−0.152 421	−0.108 522	−0.148 625	−0.152 130
$\tilde{C}_{^1S_0}^{(np)}$	−0.112 927	−0.150 034	−0.152 630	−0.108 522	−0.149 167	−0.152 327
$\tilde{C}_{^1S_0}^{(pp)}$	−0.112 927	−0.149 336	−0.151 775	−0.108 522	−0.148 236	−0.151 463
$\tilde{C}_{^3S_1}$	−0.087 340	−0.152 884	−0.166 118	−0.068 444	−0.147 784	−0.158 592
$C_{^1S_0}$	–	+1.438 619	+2.391 093	–	+1.479 889	+2.394 670
$C_{^3S_1}$	–	−0.684 095	+0.446 631	–	−0.692 660	+0.426 020
$C_{^1P_1}$	–	+0.305 070	+0.150 981	–	+0.304 204	+0.160 280
$C_{^3P_0}$	–	+1.207 031	+0.909 408	–	+1.225 764	+0.949 224
$C_{^3P_1}$	–	−0.386 920	−0.967 768	–	−0.385 154	−0.923 166
$C_{^3P_2}$	–	−0.167 769	−0.696 173	–	−0.137 914	−0.681 166
$C_{^3S_1-^3D_1}$	–	+0.132 948	+0.372 585	–	+0.133 834	+0.368 968
c_D	–	–	+1.790	–	–	+0.400
c_E	–	–	+0.130	–	–	−0.270

values (in MeV): $M_{\pi^\pm} = 139.57018$, $M_{\pi^0} = 134.9766$, $M_p = 938.272046$, $M_n = 939.565379$, $M_N = 938.918267$, and $M_\Delta = 1232$, respectively.

The statistical error from the Roy-Steiner analysis of the πN scattering data, documented in Ref. [37], as well as uncertainties because of the fit of the contact potentials, are not considered any further in this work. When contrasted with the much larger systematic uncertainties from the truncation of the EFT, such statistical errors presently play a lesser role [20,50,51]. It is important to note that although the πN LECs are extracted from πN data using a high-precision Roy-Steiner analysis, the corresponding LECs in the Δ-full sector are less precise because of the large uncertainty in the underlying determination of h_A.

To provide a crude estimate of the EFT-truncation uncertainty we follow Refs. [17,52] and write the EFT expansion for an observable X as $X = X_0 \sum_{n=0}^{\infty} a_n Q^n$. Here X_0 is the scale of the observable, given, e.g., by the LO prediction, a_n are dimensionless expansion coefficients (with $a_1 = 0$ in Weinberg power counting), and $Q \equiv p/\Lambda_b$ is the ratio of the typical momentum p and the breakdown momentum Λ_b. The application of Bayes theorem with boundless and uniform prior distribution of the expansion coefficients a_n leads to an expression for the truncation error at order NjLO ($j = 0$: LO, $j = 1$: NLO, $j = 2$: NNLO) according to

$$\sigma_X(\text{NjLO}) = X_0 Q^{j+2} \max(|a_0|, |a_1|, \ldots, |a_{j+1}|); \qquad (1)$$

see Eq. (36) of Ref. [52]. This estimate is in semiquantitative agreement with a Bayesian uncertainty quantification of the truncation error. The uncertainty at LO is further constrained to at least the size of the contribution of the higher chiral orders. For the breakdown scale Λ_b, we start from Ref. [17] but use a more conservative estimate of $\Lambda_b = 500$ MeV. We also estimate the typical momentum scale for bound state observables as $p \sim m_\pi$, and employ $p \sim p_F$ (the Fermi momentum) for infinite nucleonic matter, whereas for NN scattering we extract the momentum scale $\max(p_{\text{rel}}, m_\pi)/\Lambda$. We disregard detailed numerical factors in the various possible definitions of the relevant momentum scales for bound states because the estimate in Eq. (1) is only valid up to factors of order unity.

In Figs. 2, 3, and 4 we compare the quality of the NN scattering phase shifts of the Δ-full and Δ-less interactions with cutoff $\Lambda = 450$ MeV. The results for the peripheral waves agree well with published interactions that were analyzed in the Born approximation [31]. The dashed lines show the Δ-less results, order by order from red to green to blue. The full lines show the Δ-full results, and we remind the reader that LO is not affected by the Δ (see Fig. 1).

Clearly, in several partial waves the Δ-full χEFT interactions exhibit a faster order-by-order convergence than the corresponding Δ-less formulations. Somewhat surprisingly, the ΔNNLO results at higher scattering energies, in particular for $^1S_0$ and selected peripheral waves, such as $^1D_2$, are slightly less accurate than the corresponding Δ-less order. A more involved optimization strategy, such as Bayesian parameter estimation, could further illuminate this point. Nevertheless, the Granada phase shifts fall on the envelope of the estimated truncation errors and the results therefore seem reasonable.

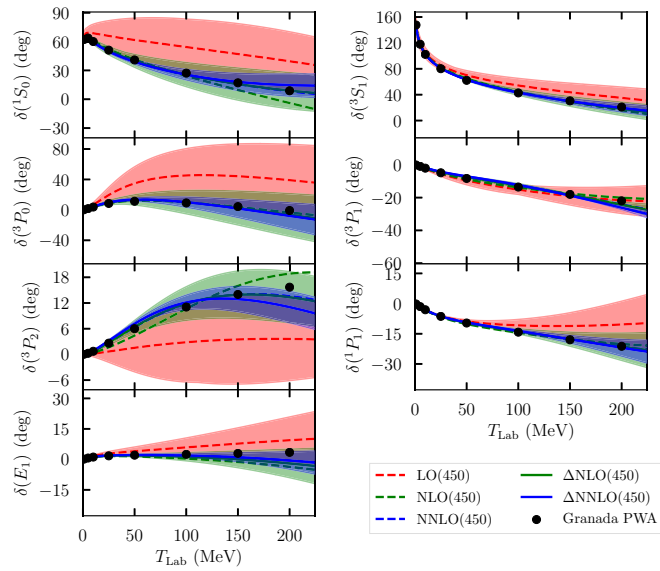

FIG. 2. Neutron-proton scattering phase shifts for the contact partial waves using the Δ-full and Δ-less χEFT potentials with nonlocal cutoff $\Lambda = 450$ MeV. All phases are compared to the results from the Granada phase shift analysis [43]. The bands correspond to the order-by-order EFT truncation error in the Δ-full approach, as described in the main text.

Although not shown, the computed phase shifts for the $\Lambda = 500$ MeV interactions are very similar and exhibit the same features.

Tables III and IV summarize our results for selected bound-state observables in $A \leqslant 4$ nuclei computed with a

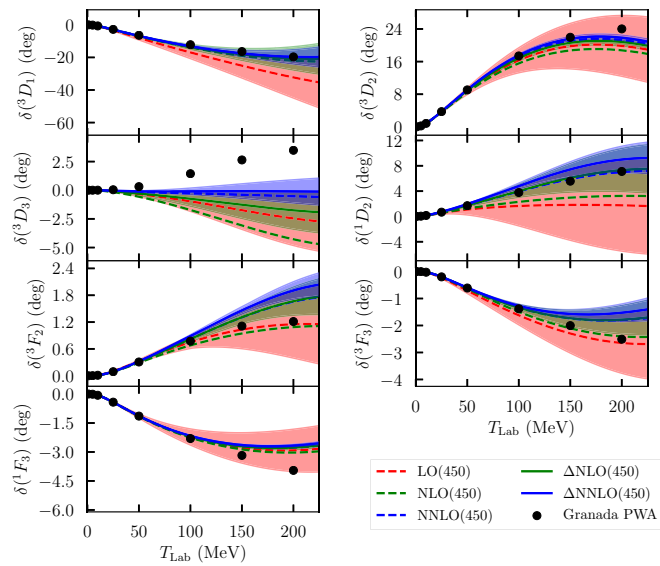

FIG. 3. Neutron-proton scattering phase shifts for selected peripheral partial waves using the Δ-full and Δ-less χEFT potentials with nonlocal cutoff $\Lambda = 450$ MeV. All phases are compared to the results from the Granada phase shift analysis [43]. The bands correspond to the order-by-order EFT truncation error in the Δ-full approach, as described in the main text.

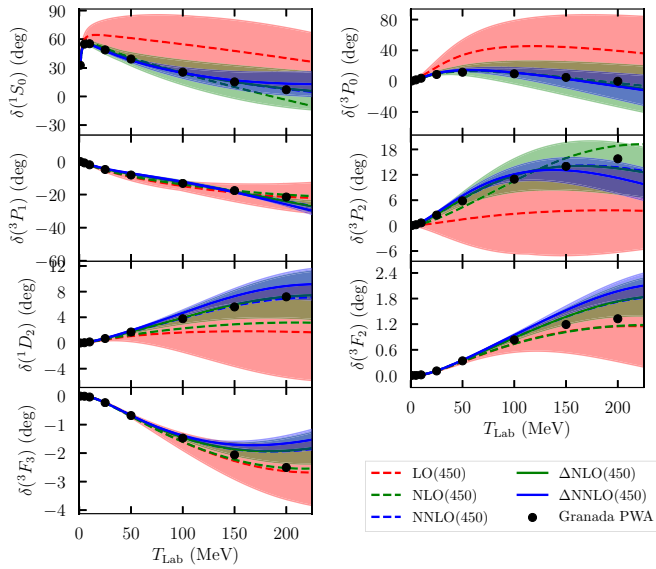

FIG. 4. Proton-proton scattering phase shifts for the contact and selected peripheral partial waves using the Δ-full and Δ-less χEFT potentials with nonlocal cutoff $\Lambda = 450$ MeV. All phases are compared to the results from the Granada phase shift analysis [43]. The bands correspond to the order-by-order EFT truncation error in the Δ-full approach, as described in the main text.

Jacobi-coordinate version [53] of the no-core shell model (NCSM) [3,4]. All calculations are converged in 41 and 21 major oscillator shells with $\hbar\Omega = 36$ MeV for $A = 3$ and $A = 4$, respectively. The charge radius and binding energy of ^{4}He were used to constrain the LECs c_D and c_E of the short-ranged three-nucleon force whereas the NCSM results for $A = 2,3$ nuclei are predictions. At NNLO, all results except the binding energy of ^{2}H, agree with the experimental values within the estimated EFT-truncation errors. The computed point-proton radii were transformed to charge radii using a standard expression; see, e.g., Ref. [18].

III. PREDICTIONS FOR MEDIUM MASS NUCLEI AND NUCLEONIC MATTER

In this section we present results for selected finite nuclei and infinite nucleonic matter. For nucleonic matter we present results for both Δ-less and Δ-full interactions, while for finite nuclei we limit the discussion to the Δ-full interactions because the Δ-less interactions produce nuclei that are not bound with respect to breakup into α particles. The computed binding energies and radii of finite nuclei are consistent with our results for the saturation point in symmetric nuclear matter.

A. Finite nuclei

The many-body calculations for finite nuclei are performed with the coupled-cluster (CC) method [5,55–57]. We employ the translationally invariant Hamiltonian,

$$H = T - T_{\rm cm} + V_{NN} + V_{NNN}. \quad (2)$$

Here, T denotes the total kinetic energy and $T_{\rm cm}$ the kinetic energy of the center of mass. As the Hamiltonian (2) does not reference the center-of-mass coordinate, the ground-state wave function is a product of an intrinsic and a Gaussian center-of-mass wave function [8,58–61]. The CC method yields a similarity transformed Hamiltonian whose ground state is the product state corresponding to a closed-shell nucleus. In the coupled-cluster singles and doubles (CCSD) approximation, typically accounting for about 90% of the correlation energy, the ground state is orthogonal to all one-particle–one-hole ($1p$-$1h$) and $2p$-$2h$ excitations. In addition to the CCSD approximation we include leading-order $3p$-$3h$ excitations perturbatively by employing the Λ-CCSD(T) method [59,62,63]. This approximation typically captures about 99% of the correlation energy. We employ a model space of 15 oscillator shells with $\hbar\Omega = 16$ MeV, and a cutoff $E_{3\rm max} = 16\hbar\Omega$ for the maximum excitation energy of three nucleons interacting via the three-nucleon potential V_{NNN}. This potential enters the CC calculations in the normal-ordered two-body approximation [64,65] in the Hartree-Fock basis.

TABLE III. Binding energies (E) in MeV, charge radii ($R_{\rm ch}$) in fm, for ^{2,3}H and ^{3,4}He at LO, NLO, and NNLO with $\Lambda = 450$ MeV, with and without the Δ isobar and compared to experiment. For the ground state of ^{2}H we also present the quadrupole moment (Q) in e fm^2 and the D-state probability ($P_{\rm D}$) in %. Experimental charge radii are from Ref. [54]. Estimates of the EFT truncation errors are given in parenthesis, and at LO we report the truncation error belonging to the Δ-full expansion.

	LO(450)	NLO(450)	ΔNLO(450)	NNLO(450)	ΔNNLO(450)	Expt.
$E(^2\text{H})$	2.01(15)	2.02(12)	2.10(5)	2.14(3)	2.16(2)	2.2245
$R_{\rm ch}(^2\text{H})$	2.16(16)	2.167(16)	2.156(7)	2.1511(44)	2.1486(19)	2.1421(88)
$P_{\rm D}(^2\text{H})$	7.15(3.51)	3.43(1.02)	3.63(97)	3.70(28)	3.74(27)	–
$Q(^2\text{H})$	0.322(41)	0.276(13)	0.277(11)	0.277(3)	0.277(3)	0.27[a]
$E(^3\text{H})$	10.91(2.38)	8.54(65)	8.65(62)	8.56(18)	8.53(17)	8.48
$R_{\rm ch}(^3\text{H})$	1.52(23)	1.70(5)	1.72(6)	1.74(1)	1.74(2)	1.7591(363)
$E(^3\text{He})$	9.95(2.21)	7.78(60)	7.85(58)	7.78(16)	7.73(16)	7.72
$R_{\rm ch}(^3\text{He})$	1.66(32)	1.91(7)	1.94(8)	1.96(2)	1.97(2)	1.9661(30)
$E(^4\text{He})$	39.60(11.3)	30.10(2.62)	29.32(2.83)	28.30(72)	28.29(78)	28.30
$R_{\rm ch}(^4\text{He})$	1.37(30)	1.59(9)	1.63(7)	1.68(3)	1.67(2)	1.6755(28)

[a]CD-Bonn value [22].

TABLE IV. Binding energies (E) in MeV, charge radii (R_{ch}) in fm, for ^{2,3}H and ^{3,4}He at LO, NLO, and NNLO with $\Lambda = 500$ MeV, with and without the Δ isobar and compared to experiment. For the ground state of ^{2}H we also present the quadrupole moment (Q) in e fm^2 and the D-state probability (P_D) in %. Experimental charge radii are from Ref. [54]. Estimates of the EFT truncation errors given in the parenthesis, and at LO we report the truncation error belonging to the Δ-full expansion.

	LO(500)	NLO(500)	ΔNLO(500)	NNLO(500)	ΔNNLO(500)	Expt.
$E(^2\mathrm{H})$	2.04(16)	2.04(12)	2.12(5)	2.16(3)	2.18(2)	2.2245
$R_{ch}(^2\mathrm{H})$	2.15(16)	2.164(16)	2.153(7)	2.149(4)	2.1459(19)	2.1421(88)
$P_D(^2\mathrm{H})$	7.80(3.97)	3.55(1.17)	3.82(1.09)	3.93(32)	3.97(30)	–
$Q(^2\mathrm{H})$	0.317(42)	0.273(12)	0.276(11)	0.275(3)	0.276(3)	0.27[a]
$E(^3\mathrm{H})$	10.47(1.97)	8.42(56)	8.91(43)	8.49(16)	8.50(12)	8.48
$R_{ch}(^3\mathrm{H})$	1.54(21)	1.71(5)	1.71(5)	1.75(1)	1.75(1)	1.7591(363)
$E(^3\mathrm{He})$	9.50(1.80)	7.66(51)	8.11(40)	7.72(14)	7.70(11)	7.72
$R_{ch}(^3\mathrm{He})$	1.68(30)	1.93(7)	1.92(7)	1.97(2)	1.98(2)	1.9661(30)
$E(^4\mathrm{He})$	37.00(8.69)	29.22(2.15)	30.70(2.38)	28.31(60)	28.31(65)	28.30
$R_{ch}(^4\mathrm{He})$	1.39(28)	1.60(7)	1.62(6)	1.68(2)	1.67(2)	1.6755(28)

[a]CD-Bonn value [22].

To assess the impact of the Δ isobar in finite nuclei we calculated the binding energies and charge radii for ^{4}He, ^{16}O, and ^{40}Ca order-by-order, i.e., at LO, NLO, and NNLO. Figure 5 shows the results using the Δ-full interactions with a momentum cutoff $\Lambda = 450$ MeV. The ground-state energies are $E(^{16}\mathrm{O}) = -108.8(11.4)$, $-120.3(6.4)$, and $-117.0(1.8)$ MeV and $E(^{40}\mathrm{Ca}) = -216(97)$, $-312(52)$, and $-309(14)$ MeV at LO, NLO, and NNLO, respectively. The charge radii are $R_{ch}(^{16}\mathrm{O}) = 1.96(0.76)$, 2.63(0.36), and 2.73(0.10) fm and $R_{ch}(^{40}\mathrm{Ca}) = 2.29(1.25)$, 3.41(0.61), and 3.55(0.17) fm at LO, NLO, and NNLO, respectively. Before we analyze the results, we estimate the systematic uncertainties from the truncation of the EFT. Again we follow Refs. [17,66], use Eq. (1), and set the momentum scale $p = m_\pi$ for our low-energy observables. The predicted charge radii are accurate at each order within

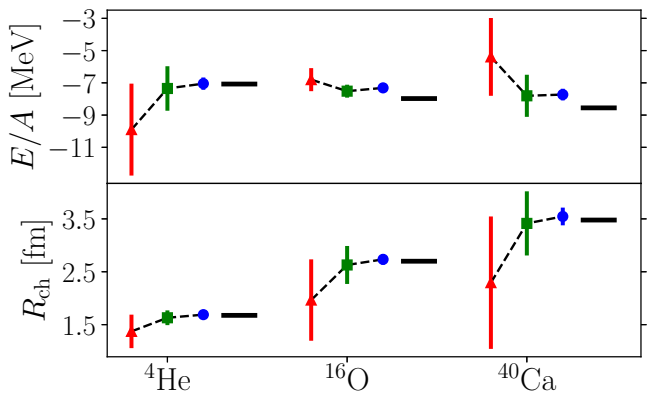

FIG. 5. Ground-state energy (negative of binding energy) per nucleon and charge radii for selected nuclei computed with coupled cluster theory and the Δ-full potential ($\Lambda = 450$ MeV). For each nucleus, from left to right as follows: LO (red triangle), NLO (green square), and NNLO (blue circle). The black bars are data. Vertical bars estimate uncertainties from the order-by-order EFT truncation errors σ(LO), σ(NLO), and σ(NNLO). At NLO and NNLO we estimate a conservative 95% confidence interval, i.e., $1.96 \times \sigma$. See the text for details.

uncertainties. Already at NLO, which is independent of the subleading 2π-exchange LECs c_i, we obtain an accurate description of both radii and binding energies of ^{4}He, ^{16}O, and ^{40}Ca. At NNLO, the charge radii also exhibit a first sign of convergence in terms of the chiral expansion. Binding energies exhibit a nearly identical order-by-order increase in precision but somewhat underbind nuclei at NNLO. These results demonstrate that the Δ isobar can play an important role also in low-energy nuclear structure and nuclear saturation [14,50].

The Δ degree of freedom also impacts the stability of nuclei with respect to breakup into alpha particles. At LO, ^{16}O and ^{40}Ca are not stable with respect to alpha emission. Similar results were observed in pionless EFT [67–69] and nuclear lattice EFT [25]. However, the Δ modifies the 2π exchanges between nucleons, and we observe that the Δ-full interactions at NLO and NNLO yield nuclei that are stable with respect to alpha emission. This is in stark contrast to results we obtained here using the Δ-less NLO and NNLO interactions at cutoff $\Lambda = 450$ MeV, and to those of Ref. [20].

Table V summarizes binding energies, radii, and also the neutron skins of nuclei with closed subshells up to ^{48}Ca. Note that the lack of a spin-orbit (LS) force at LO results in energy degeneracies that hamper CC calculations of non-LS-closed nuclei. Therefore, we can obtain EFT truncation errors only for ^{16}O and ^{40}Ca using Eq. (1). For ^{48}Ca we predict a neutron skin of $R_{skin} = 0.15$ fm at ΔNLO and ΔNNLO, consistent with the recent ranges 0.14–0.20 fm and 0.12–0.15 fm from Ref. [70] and Ref. [7], respectively.

Figure 6 shows the charge form factor at ΔNLO and ΔNNLO, compared to NNLO$_{sat}$ [18] and data. The charge form factor is obtained by a Fourier transform of the intrinsic charge density [7,72], and agrees with data for momentum transfers up to about $q \approx 2.5$ fm^{-1}. Also for this quantity, the ΔNLO results indicate an improved convergence of chiral expansion compared to the Δ-less formulation.

We also computed spectra of various nuclei. These explorations exhibited mixed results: While the low-lying states in ^{17}O were in good agreement with data, ^{25}O is bound at ΔNNLO

TABLE V. Binding energies (E) (in MeV), charge radii (in fm), proton point radii (in fm), neutron point radii (in fm), and neutron skin (in fm) for ^{8}He, ^{16,22,24}O, and ^{40,48}Ca at ΔNLO and ΔNNLO, and compared to experiment.

	E			$R_{\rm ch}$			$R_{\rm p}$		$R_{\rm n}$		$R_{\rm skin}$	
	ΔNLO	ΔNNLO	Expt. [71]	ΔNLO	ΔNNLO	Expt. [54]	ΔNLO	ΔNNLO	ΔNLO	ΔNNLO	ΔNLO	ΔNNLO
^{8}He	27.5	27.0	31.40	1.90	1.97	1.924(31)	1.77	1.85	2.63	2.70	0.85	0.85
^{16}O	120.3	117.0	127.62	2.63	2.73	2.699(5)	2.49	2.61	2.47	2.58	−0.02	−0.03
^{22}O	146.2	145.4	162.04	2.66	2.77		2.54	2.66	2.88	3.00	0.34	0.34
^{24}O	152.2	151.6	168.96	2.70	2.81		2.59	2.71	3.11	3.22	0.52	0.51
^{40}Ca	312.2	309.1	342.05	3.41	3.55	3.478(2)	3.31	3.45	3.26	3.40	−0.05	−0.05
^{48}Ca	373.4	373.8	416.00	3.45	3.56	3.477(2)	3.36	3.47	3.51	3.62	0.15	0.15

with respect to ^{24}O by about 0.5 MeV, and the $J^{\pi} = 2^{+}$ state in ^{24}O is too low. We believe that these shortcomings should not distract from the main results reported in this work: accurate saturation properties at NLO in the Δ-full χEFT. We speculate that finer details such as spectra will require us to go to higher order in the *NN* interaction (as was done, e.g., in Ref. [34] by including N^{3}LO contacts), or to vary the Δ-full πN couplings within their somewhat more generous uncertainty limits because of the somewhat poorly known $\pi N\Delta$ coupling h_A, or to also use data of heavier nuclei in the optimization of the interaction. The interactions constructed in this work serve as excellent starting points for such endeavors.

B. Nucleonic matter

We turn to the CC calculations of nuclear matter using Δ-full and Δ-less interactions up to NNLO. We follow Ref. [73] and employ a Hamiltonian $H = T + V_{NN} + V_{NNN}$. The basis is a discrete lattice in momentum space corresponding to periodic boundary conditions in a cubic box of length L in position space, and the discrete lattice momenta are given by $2\pi\hbar n_i/L$, with $n_i = 0, \pm 1, \ldots \pm n_{\rm max}$, and $i = x,y,z$. We used $n_{\rm max} = 4$ as the maximum number of lattice points. The CC calculations were carried out at the doubles excitation level ($2p$-$2h$) with perturbative triples ($3p$-$3h$) corrections [CCD(T)]. Because of translational invariance, there are no $1p$-$1h$ excitations. We use "closed-shell" lattice configurations with 66 neutrons for neutron matter, and 132 nucleons for symmetric nuclear matter. These nucleon numbers exhibit only small finite-size effects [73,74]. The CCD(T) calculations were performed with the normal-ordered two-body approximation for the *NNN* interaction [64,65], i.e., the three-nucleon force enters the normal-ordered Hamiltonian as 0-body, 1-body, and 2-body interactions; summing over 3, 2, and 1 particles in the reference state, respectively. All results are well converged for $n_{\rm max} = 4$ at all considered densities, i.e., $\rho \leqslant 0.2$ fm^{-3}. To gauge the quality of the normal-ordered two-body approximation, we also included the "residual" *NNN* interaction (i.e., those that generate $3p$-$3h$ excitations when acting on the reference) in perturbation theory. We found that the residual *NNN* contribution is negligible for neutron matter, and small (0.2–0.3 MeV per nucleon) in symmetric nuclear matter. This suggests that the normal-ordered two-body approximation for the three-nucleon force is sufficiently precise for the Δ-full interactions considered in this work.

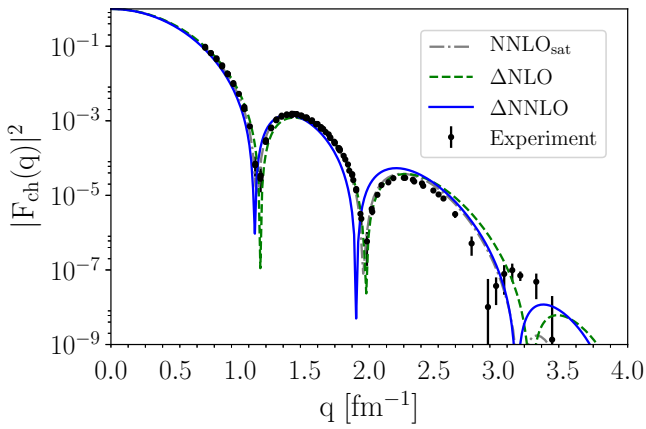

FIG. 6. Elastic charge form factor of ^{48}Ca from NNLO$_{\rm sat}$ (gray dash-dotted), ΔNLO (green dashed), and ΔNNLO (blue solid line) compared to experimental data (black).

In Fig. 7 we compare the results for the energy per nucleon at different densities in symmetric nuclear matter and pure neutron matter using Δ-full and Δ-less interactions with a momentum cutoff $\Lambda = 450$ MeV at LO, NLO, and NNLO. The saturation points in symmetric matter at NLO and NNLO shift towards considerably more realistic values upon inclusion of the Δ. This observation is consistent with our results for finite nuclei. For the EFT truncation uncertainty we use Eq. (1), a relevant momentum scale $p = p_F$, and the breakdown momentum $\Lambda_b = 500$ MeV. The uncertainties also make the accelerated convergence and consistency of the Δ-full expansion more apparent. We note that our breakdown scale Λ_b is somewhat conservative. For $\Lambda_b \gtrsim 650$ MeV the truncation-error bands of the Δ-full and Δ-less NNLO(450) interactions no longer overlap in the region of the empirical saturation density. We also note that nuclear matter does not saturate at LO in the range of densities we studied, and we remind the reader once more that the Δ does not enter at this chiral order.

Figure 8 shows the difference between the equations of state for neutron matter and symmetric nuclear matter for the $\Lambda = 450$ MeV cutoff. At the saturation density (ρ_0), indicated as vertical lines for the different orders, this yields the symmetry energy (S_0). Our results are $\rho_0 = 0.18(1)$ fm^{-3}, $22.8 \lesssim S_0 \lesssim 36.5$ MeV, and $46 \lesssim L \lesssim 65$ MeV at ΔNLO, and $\rho_0 = 0.165(1)$ fm^{-3}, $23.6 \lesssim S_0 \lesssim 33.3$ MeV, and

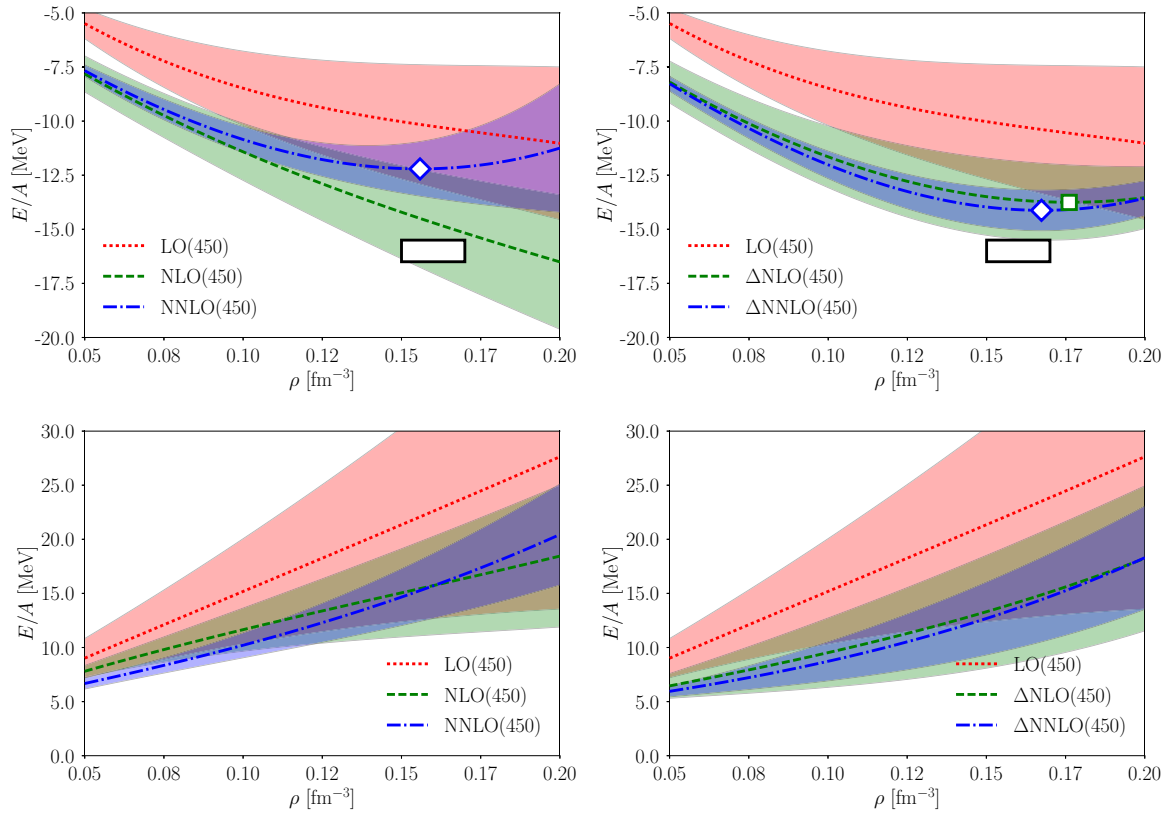

FIG. 7. Energy per nucleon (in MeV) of symmetric nuclear matter (upper row) and pure neutron matter (lower row) up to third order in χEFT without (left column) and with (right column) explicit inclusion of the Δ isobar in χEFT. All interaction employ a momentum cutoff $\Lambda = 450$ MeV. Shaded areas indicate the estimated EFT-truncation errors, and the (square) diamond marks the saturation point in symmetric nuclear matter for (ΔNLO) ΔNNLO. The black rectangle indicates the region $E/A = -16 \pm 0.5$ MeV and $\rho = 0.16 \pm 0.01$ fm^{-3}.

$32 \lesssim L \lesssim 67$ MeV at ΔNNLO. The estimated EFT truncation error for ρ_0 is very small at ΔNNLO because its central value and lower and upper bounds have essentially the same saturation point. The estimated EFT truncation error for S_0 is the maximum difference between the energies per particle in neutron matter and symmetric nuclear matter, at the saturation point. This uncertainty also decreases with increasing order. Finally, the estimated uncertainty in the slope (L) of the symmetry energy is taken from the ranges of slopes of S_0 at its upper and lower values. It is large even at ΔNNLO and reflects that the slope in neutron matter exhibits a greater variance at ΔNNLO than at ΔNLO; see Fig. 7. We note that our predictions for the symmetry energy and its density derivative at ΔNLO and ΔNNLO are consistent with the recent estimates of Refs. [75,76].

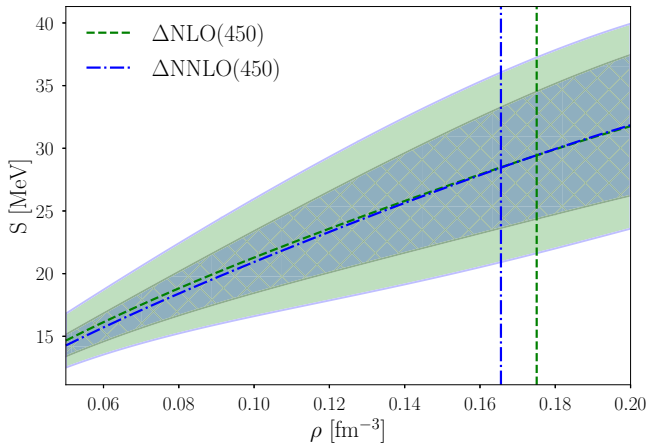

FIG. 8. The symmetry energy as a function of the density for ΔNLO (green), and ΔNNLO (blue) with Δ-full interaction at cutoff of 450 MeV, with uncertainties shown as shaded areas.

IV. SUMMARY

We presented results for selected finite nuclei and infinite nucleonic matter using optimized interactions from χEFT with explicit Δ-isobar degree of freedom. We optimized both Δ-full and Δ-less interactions order by order in the power counting up to NNLO, for two different cutoffs, and with πN LECs from a recent Roy-Steiner analysis of πN scattering. The NN contact potentials up to NNLO were adjusted to NN phase shifts, while the short-ranged parts of the NNN interactions were constrained by energy and radius data on ^{4}He. We emphasize that the only differences between the Δ-full and Δ-less interactions are because of the explicit inclusion of the Δ isobar. In a detailed comparison, we found that radii in nuclei up to ^{48}Ca are accurate within EFT-truncation error estimates, and that binding energies—while improving order

by order in precision—somewhat underbind heavier nuclei. The saturation point in nuclear matter is consistent with data within EFT error estimates. Our results also show that the inclusion of Δ isobars in the nuclear interaction can address the long-standing problem regarding nuclear saturation. This work therefore provides a valuable starting point for constructing more refined Δ-full χEFT interactions, also at higher chiral orders, with improved uncertainty estimates.

ACKNOWLEDGMENTS

We would like to thank Hermann Krebs for valuable discussions and input on the manuscript, Kai Hebeler for providing us with matrix elements in Jacobi coordinates for the three-nucleon interaction, and Gustav Jansen for providing us with the code that transforms three-nucleon matrix elements to the laboratory system. This material is based upon work supported by the Swedish Research Council under Grant No. 2015-00225, and the Marie Sklodowska Curie Actions, Cofund, Project No. INCA 600398, the US Department of Energy, Office of Science, Office of Nuclear Physics under Grants No. DEFG02-96ER40963 (University of Tennessee), No. DE-SC0008499, and No. DE-SC0018223 (NUCLEI SciDAC collaboration), and the Field Work Proposal ERKBP57 at Oak Ridge National Laboratory. Computer time was provided by the Innovative and Novel Computational Impact on Theory and Experiment (INCITE) program. This research used resources of the Oak Ridge Leadership Computing Facility located in the Oak Ridge National Laboratory, which is supported by the Office of Science of the Department of Energy under Contract No. DE-AC05-00OR22725, and used computational resources of the National Center for Computational Sciences, the National Institute for Computational Sciences, and the Swedish National Infrastructure for Computing (SNIC) project SNIC 2016/1-157.

The United States Government retains and the publisher, by accepting the article for publication, acknowledges that the United States Government retains a nonexclusive, paid-up, irrevocable, worldwide license to publish or reproduce the published form of this manuscript, or allow others to do so, for United States Government purposes. The Department of Energy will provide public access to these results of federally sponsored research in accordance with the DOE Public Access Plan (http://energy.gov/downloads/doe-public-access-plan).

[1] H. Kamada, A. Nogga, W. Glöckle, E. Hiyama, M. Kamimura, K. Varga, Y. Suzuki, M. Viviani, A. Kievsky, S. Rosati, J. Carlson, Steven C. Pieper, R. B. Wiringa, P. Navrátil, B. R. Barrett, N. Barnea, W. Leidemann, and G. Orlandini, Benchmark test calculation of a four-nucleon bound state, Phys. Rev. C **64**, 044001 (2001).

[2] S. C. Pieper and R. B. Wiringa, Quantum Monte Carlo calculations of light nuclei, Ann. Rev. Nucl. Part. Sci. **51**, 53 (2001).

[3] P. Navrátil, S. Quaglioni, I. Stetcu, and B. R. Barrett, Recent developments in no-core shell-model calculations, J. Phys. G: Nucl. Part. Phys. **36**, 083101 (2009).

[4] B. R. Barrett, P. Navrátil, and J. P. Vary, Ab initio no core shell model, Prog. Part. Nucl. Phys. **69**, 131 (2013).

[5] G. Hagen, T. Papenbrock, M. Hjorth-Jensen, and D. J. Dean, Coupled-cluster computations of atomic nuclei, Rep. Prog. Phys. **77**, 096302 (2014).

[6] T. A. Lähde, E. Epelbaum, H. Krebs, D. Lee, U.-G. Meißner, and G. Rupak, Lattice effective field theory for medium-mass nuclei, Phys. Lett. B **732**, 110 (2014).

[7] G. Hagen, A. Ekström, C. Forssén, G. R. Jansen, W. Nazarewicz, T. Papenbrock, K. A. Wendt, S. Bacca, N. Barnea, B. Carlsson, C. Drischler, K. Hebeler, M. Hjorth-Jensen, M. Miorelli, G. Orlandini, A. Schwenk, and J. Simonis, Neutron and weak-charge distributions of the ^{48}Ca nucleus, Nat. Phys. **12**, 186 (2016).

[8] H. Hergert, S. K. Bogner, T. D. Morris, A. Schwenk, and K. Tsukiyama, The in-medium similarity renormalization group: A novel ab initio method for nuclei, Phys. Rep. **621**, 165 (2016).

[9] G. Hagen, G. R. Jansen, and T. Papenbrock, Structure of ^{78}Ni from First-Principles Computations, Phys. Rev. Lett. **117**, 172501 (2016).

[10] E. Epelbaum, W. Glöckle, and U.-G. Meißner, Nuclear forces from chiral Lagrangians using the method of unitary transformation II: The two-nucleon system, Nucl. Phys. A **671**, 295 (2000).

[11] E. Epelbaum, A. Nogga, W. Glöckle, H. Kamada, Ulf-G. Meißner, and H. Witała, Three-nucleon forces from chiral effective field theory, Phys. Rev. C **66**, 064001 (2002).

[12] D. R. Entem and R. Machleidt, Accurate charge-dependent nucleon-nucleon potential at fourth order of chiral perturbation theory, Phys. Rev. C **68**, 041001 (2003).

[13] A. M. Shirokov, A. I. Mazur, S. A. Zaytsev, J. P. Vary, and T. A. Weber, Nucleon-nucleon interaction in the j-matrix inverse scattering approach and few-nucleon systems, Phys. Rev. C **70**, 044005 (2004).

[14] K. Hebeler, S. K. Bogner, R. J. Furnstahl, A. Nogga, and A. Schwenk, Improved nuclear matter calculations from chiral low-momentum interactions, Phys. Rev. C **83**, 031301 (2011).

[15] A. Ekström, G. Baardsen, C. Forssén, G. Hagen, M. Hjorth-Jensen, G. R. Jansen, R. Machleidt, W. Nazarewicz, T. Papenbrock, J. Sarich, and S. M. Wild, Optimized Chiral Nucleon-Nucleon Interaction at Next-to-Next-to-Leading Order, Phys. Rev. Lett. **110**, 192502 (2013).

[16] D. R. Entem, N. Kaiser, R. Machleidt, and Y. Nosyk, Peripheral nucleon-nucleon scattering at fifth order of chiral perturbation theory, Phys. Rev. C **91**, 014002 (2015).

[17] E. Epelbaum, H. Krebs, and U.-G. Meißner, Precision Nucleon-Nucleon Potential at Fifth Order in the Chiral Expansion, Phys. Rev. Lett. **115**, 122301 (2015).

[18] A. Ekström, G. R. Jansen, K. A. Wendt, G. Hagen, T. Papenbrock, B. D. Carlsson, C. Forssén, M. Hjorth-Jensen, P. Navrátil, and W. Nazarewicz, Accurate nuclear radii and binding energies from a chiral interaction, Phys. Rev. C **91**, 051301 (2015).

[19] J. E. Lynn, I. Tews, J. Carlson, S. Gandolfi, A. Gezerlis, K. E. Schmidt, and A. Schwenk, Chiral Three-Nucleon Interactions in Light Nuclei, Neutron-α Scattering, and Neutron Matter, Phys. Rev. Lett. **116**, 062501 (2016).

[20] B. D. Carlsson, A. Ekström, C. Forssén, D. F. Strömberg, G. R. Jansen, O. Lilja, M. Lindby, B. A. Mattsson, and K.

A. Wendt, Uncertainty Analysis and Order-by-Order Optimization of Chiral Nuclear Interactions, Phys. Rev. X **6**, 011019 (2016).
[21] E. Epelbaum, H.-W. Hammer, and U.-G. Meißner, Modern theory of nuclear forces, Rev. Mod. Phys. **81**, 1773 (2009).
[22] R. Machleidt and D. R. Entem, Chiral effective field theory and nuclear forces, Phys. Rep. **503**, 1 (2011).
[23] S. Binder, J. Langhammer, A. Calci, and R. Roth, Ab initio path to heavy nuclei, Phys. Lett. B **736**, 119 (2014).
[24] J. Simonis, S. R. Stroberg, K. Hebeler, J. D. Holt, and A. Schwenk, Saturation with chiral interactions and consequences for finite nuclei, Phys. Rev. C **96**, 014303 (2017).
[25] S. Elhatisari, N. Li, A. Rokash, J. M. Alarcón, D. Du, N. Klein, B.-N. Lu, Ulf-G. Meißner, E. Epelbaum, H. Krebs, T. A. Lähde, D. Lee, and G. Rupak, Nuclear Binding Near a Quantum Phase Transition, Phys. Rev. Lett. **117**, 132501 (2016).
[26] U. van Kolck, Few-nucleon forces from chiral Lagrangians, Phys. Rev. C **49**, 2932 (1994).
[27] C. Ordóñez, L. Ray, and U. van Kolck, Nucleon-Nucleon Potential from an Effective Chiral Lagrangian, Phys. Rev. Lett. **72**, 1982 (1994).
[28] C. Ordóñez, L. Ray, and U. van Kolck, Two-nucleon potential from chiral Lagrangians, Phys. Rev. C **53**, 2086 (1996).
[29] V. Bernard, N. Kaiser, and U.-G. Meißner, Aspects of chiral pion-nucleon physics, Nucl. Phys. A **615**, 483 (1997).
[30] M. Piarulli, L. Girlanda, R. Schiavilla, R. N. Pérez, J. E. Amaro, and E. R. Arriola, Minimally nonlocal nucleon-nucleon potentials with chiral two-pion exchange including Δ resonances, Phys. Rev. C **91**, 024003 (2015).
[31] H. Krebs, E. Epelbaum, and U. G. Meißner, Nuclear forces with Δ excitations up to next-to-next-to-leading order, part I: Peripheral nucleon-nucleon waves, Eur. Phys. J. A **32**, 127 (2007).
[32] M. Piarulli, L. Girlanda, R. Schiavilla, A. Kievsky, A. Lovato, L. E. Marcucci, Steven C. Pieper, M. Viviani, and R. B. Wiringa, Local chiral potentials with Δ-intermediate states and the structure of light nuclei, Phys. Rev. C **94**, 054007 (2016).
[33] D. Logoteta, I. Bombaci, and A. Kievsky, Nuclear matter properties from local chiral interactions with Δ isobar intermediate states, Phys. Rev. C **94**, 064001 (2016).
[34] M. Piarulli, A. Baroni, L. Girlanda, A. Kievsky, A. Lovato, E. Lusk, L. E. Marcucci, S. C. Pieper, R. Schiavilla, M. Viviani, and R. B. Wiringa, Light-Nuclei Spectra from Chiral Dynamics, Phys. Rev. Lett. **120**, 052503 (2018).
[35] J.-I. Fujita and H. Miyazawa, Pion theory of three-body forces, Prog. Theor. Phys. **17**, 360 (1957).
[36] E. Epelbaum, H. Krebs, and U.-G. Meißner, Δ-excitations and the three-nucleon force, Nucl. Phys. A **806**, 65 (2008).
[37] D. Siemens, J. R. de Elvira, E. Epelbaum, M. Hoferichter, H. Krebs, B. Kubis, and U.-G. Meißner, Reconciling threshold and subthreshold expansions for pion-nucleon scattering, Phys. Lett. B **770**, 27 (2017).
[38] M. Hoferichter, J. Ruiz de Elvira, B. Kubis, and U.-G. Meißner, Roy-steiner-equation analysis of pion-nucleon scattering, Phys. Rept. **625**, 1 (2016).
[39] T. R. Hemmert, B. R. Holstein, and J. Kambor, Heavy baryon chiral perturbation theory with light deltas, J. Phys. G: Nucl. Part. Phys. **24**, 1831 (1998).
[40] N. Kaiser, S. Gerstendörfer, and W. Weise, Peripheral NN-scattering: role of delta-excitation, correlated two-pion and vector meson exchange, Nucl. Phys. A **637**, 395 (1998).
[41] B. Long and V. Lensky, Heavy-particle formalism with Foldy-Wouthuysen representation, Phys. Rev. C **83**, 045206 (2011).
[42] V. R. Pandharipande, D. R. Phillips, and U. van Kolck, Δ effects in pion-nucleon scattering and the strength of the two-pion-exchange three-nucleon interaction, Phys. Rev. C **71**, 064002 (2005).
[43] R. N. Pérez, J. E. Amaro, and E. R. Arriola, Coarse-grained potential analysis of neutron-proton and proton-proton scattering below the pion production threshold, Phys. Rev. C **88**, 064002 (2013).
[44] E. Epelbaum, W. Glöckle, and U.-G. Meißner, The two-nucleon system at next-to-next-to-next-to-leading order, Nucl. Phys. A **747**, 362 (2005).
[45] M. P. Valderrama and E. R. Arriola, Renormalization of chiral two-pion exchange *NN* interactions with Δ excitations: Central phases and the deuteron, Phys. Rev. C **79**, 044001 (2009).
[46] M. Pavon Valderrama and E. Ruiz Arriola, Renormalization of chiral two-pion exchange *NN* interactions with Δ excitations: Correlations in the partial-wave expansion, Phys. Rev. C **83**, 044002 (2011).
[47] E. Epelbaum, H. Krebs, and U. G. Meißner, Improved chiral nucleon-nucleon potential up to next-to-next-to-next-to-leading order, Eur. Phys. J. A **51**, 53 (2015).
[48] A. Dyhdalo, R. J. Furnstahl, K. Hebeler, and I. Tews, Regulator artifacts in uniform matter for chiral interactions, Phys. Rev. C **94**, 034001 (2016).
[49] J. Hoppe, C. Drischler, R. J. Furnstahl, K. Hebeler, and A. Schwenk, Weinberg eigenvalues for chiral nucleon-nucleon interactions, Phys. Rev. C **96**, 054002 (2017).
[50] A. Ekström, B. D. Carlsson, K. A. Wendt, C. Forssén, M. Hjorth Jensen, R. Machleidt, and S. M. Wild, Statistical uncertainties of a chiral interaction at next-to-next-to leading order, J. Phys. G **42**, 034003 (2015).
[51] R. N. Pérez, J. E. Amaro, and E. R. Arriola, Low-energy chiral two-pion exchange potential with statistical uncertainties, Phys. Rev. C **91**, 054002 (2015).
[52] R. J. Furnstahl, N. Klco, D. R. Phillips, and S. Wesolowski, Quantifying truncation errors in effective field theory, Phys. Rev. C **92**, 024005 (2015).
[53] P. Navrátil, G. P. Kamuntavičius, and B. R. Barrett, Few-nucleon systems in a translationally invariant harmonic oscillator basis, Phys. Rev. C **61**, 044001 (2000).
[54] I. Angeli and K. P. Marinova, Table of experimental nuclear ground state charge radii: An update, At. Data Nucl. Data Tables **99**, 69 (2013).
[55] H. Kümmel, K. H. Lührmann, and J. G. Zabolitzky, Many-fermion theory in exp *S* (or coupled cluster) form, Phys. Rep. **36**, 1 (1978).
[56] R. F. Bishop, An overview of coupled cluster theory and its applications in physics, Theor. Chim. Acta **80**, 95 (1991).
[57] R. J. Bartlett and M. Musiał, Coupled-cluster theory in quantum chemistry, Rev. Mod. Phys. **79**, 291 (2007).
[58] G. Hagen, T. Papenbrock, and D. J. Dean, Solution of the Center-of-Mass Problem in Nuclear Structure Calculations, Phys. Rev. Lett. **103**, 062503 (2009).
[59] G. Hagen, T. Papenbrock, D. J. Dean, and M. Hjorth-Jensen, *Ab initio* coupled-cluster approach to nuclear structure with modern nucleon-nucleon interactions, Phys. Rev. C **82**, 034330 (2010).
[60] G. R. Jansen, Spherical coupled-cluster theory for open-shell nuclei, Phys. Rev. C **88**, 024305 (2013).

[61] T. D. Morris, N. M. Parzuchowski, and S. K. Bogner, Magnus expansion and in-medium similarity renormalization group, Phys. Rev. C **92**, 034331 (2015).

[62] A. G. Taube and R. J. Bartlett, Improving upon CCSD(T): Lambda CCSD(T). I. potential energy surfaces, J. Chem. Phys. **128**, 044110 (2008).

[63] S. Binder, P. Piecuch, A. Calci, J. Langhammer, P. Navrátil, and R. Roth, Extension of coupled-cluster theory with a noniterative treatment of connected triply excited clusters to three-body Hamiltonians, Phys. Rev. C **88**, 054319 (2013).

[64] G. Hagen, T. Papenbrock, D. J. Dean, A. Schwenk, A. Nogga, M. Włoch, and P. Piecuch, Coupled-cluster theory for three-body Hamiltonians, Phys. Rev. C **76**, 034302 (2007).

[65] R. Roth, S. Binder, K. Vobig, A. Calci, J. Langhammer, and P. Navrátil, Medium-Mass Nuclei with Normal-Ordered Chiral $NN+3N$ Interactions, Phys. Rev. Lett. **109**, 052501 (2012).

[66] S. Binder, A. Calci, E. Epelbaum, R. J. Furnstahl, J. Golak, K. Hebeler, H. Kamada, H. Krebs, J. Langhammer, S. Liebig, P. Maris, Ulf-G. Meißner, D. Minossi, A. Nogga, H. Potter, R. Roth, R. Skibiński, K. Topolnicki, J. P. Vary, and H. Witała (LENPIC Collaboration), Few-nucleon systems with state-of-the-art chiral nucleon-nucleon forces, Phys. Rev. C **93**, 044002 (2016).

[67] I. Stetcu, B. R. Barrett, and U. van Kolck, No-core shell model in an effective-field-theory framework, Phys. Lett. B **653**, 358 (2007).

[68] L. Contessi, A. Lovato, F. Pederiva, A. Roggero, J. Kirscher, and U. van Kolck, Ground-state properties of ^{4}He and ^{16}O extrapolated from lattice QCD with pionless EFT, Phys. Lett. B **772**, 839 (2017).

[69] A. Bansal, S. Binder, A. Ekström, G. Hagen, G. R. Jansen, and T. Papenbrock, arXiv:1712.10246.

[70] J. Birkhan, M. Miorelli, S. Bacca, S. Bassauer, C. A. Bertulani, G. Hagen, H. Matsubara, P. von Neumann-Cosel, T. Papenbrock, N. Pietralla, V. Yu. Ponomarev, A. Richter, A. Schwenk, and A. Tamii, Electric Dipole Polarizability of ^{48}Ca and Implications for the Neutron Skin, Phys. Rev. Lett. **118**, 252501 (2017).

[71] M. Wang, G. Audi, A. H. Wapstra, F. G. Kondev, M. MacCormick, X. Xu, and B. Pfeiffer, The AME2012 atomic mass evaluation, Chin. Phys. C **36**, 1603 (2012).

[72] B. G. Giraud, Density functionals in the laboratory frame, Phys. Rev. C **77**, 014311 (2008).

[73] G. Hagen, T. Papenbrock, A. Ekström, K. A. Wendt, G. Baardsen, S. Gandolfi, M. Hjorth-Jensen, and C. J. Horowitz, Coupled-cluster calculations of nucleonic matter, Phys. Rev. C **89**, 014319 (2014).

[74] S. Gandolfi, A. Yu. Illarionov, K. E. Schmidt, F. Pederiva, and S. Fantoni, Quantum Monte Carlo calculation of the equation of state of neutron matter, Phys. Rev. C **79**, 054005 (2009).

[75] M. B. Tsang, J. R. Stone, F. Camera, P. Danielewicz, S. Gandolfi, K. Hebeler, C. J. Horowitz, Jenny Lee, W. G. Lynch, Z. Kohley, R. Lemmon, P. Möller, T. Murakami, S. Riordan, X. Roca-Maza, F. Sammarruca, A. W. Steiner, I. Vidaña, and S. J. Yennello, Constraints on the symmetry energy and neutron skins from experiments and theory, Phys. Rev. C **86**, 015803 (2012).

[76] I. Tews, J. M. Lattimer, A. Ohnishi, and E. E. Kolomeitsev, Symmetry parameter constraints from a lower bound on the neutron-matter energy, Astrophys. J. **848**, 105 (2017).